Available online at www.sciencedirect.com
ScienceDirect
European Journal of Pharmaceutics and Biopharmaceutics 67 (2007) 339–348
European Journal of Pharmaceutics and Biopharmaceutics
www.elsevier.com/locate/ejpb

Research paper

Cross-linking of chitosan and chitosan/poly(ethylene oxide) beads: A theoretical treatment

Leticia Martinez [a], Florence Agnely [a,*], Bernard Leclerc [a], Juergen Siepmann [b], Marine Cotte [c], Sandrine Geiger [a], Guy Couarraze [a]

[a] *Faculté de Pharmacie, Université Paris-Sud, Châtenay-Malabry, France*
[b] *College of Pharmacy, University of Lille, Lille, France*
[c] *European Synchroton Radiation Facility, Grenoble, France*

Received 28 July 2006; accepted in revised form 16 February 2007
Available online 24 February 2007

Abstract

The major aim of this study was to get deeper insight into the process of polymer cross-linking and the resulting structure of beads based on chitosan (CS) or chitosan/poly(ethylene oxide) (CS/PEO) semi-interpenetrating networks (semi-IPNs) as new carrier materials for oral drug delivery. Spherical hydrogels were prepared by a dropping method. The uptake kinetics of the cross-linking agent glyoxal into the beads were monitored and quantitatively described using Fick's second law of diffusion. High-resolution synchrotron infrared microspectroscopy (SIRM) was used to characterize the inner structures of the beads. Importantly, the diffusion of glyoxal through the hydrogels was found to be much slower than the cross-linking reaction and the mesh size of the created networks to be much larger than the hydrodynamic diameter of glyoxal. The presence of PEO chains slightly decreased the diffusivity of glyoxal due to obstruction effects. However, the cross-linking reaction was not affected. Interestingly, the polymers were homogeneously cross-linked throughout the beads, except for a thin outer shell showing an elevated cross-linking density. Thus, the obtained cross-linked hydrogel-based beads exhibit well-defined polymeric structures and offer an interesting potential as novel oral drug delivery systems.

Keywords: Beads; Chitosan; Cross-linking; Diffusion; Glyoxal; Modeling; Semi-IPN, Synchrotron infrared microspectroscopy

1. Introduction

Chitosan (CS) is a natural and abundant polysaccharide obtained by N-deacetylation of chitin. Chitin is extracted from crustaceans and insect shells, algae and certain fungi. The physicochemical and biological properties of CS (such as biodegradability, biocompatibility, non-toxicity, mucoadhesion, absorption enhancement and pH-dependent swelling) are of great interest in the biomedical and pharmaceutical fields [1–6]. That is why CS networks are already used as hydrophilic matrix formers in controlled drug delivery systems [7,8].

Chemical cross-linking of CS with dialdehydes, such as glyoxal, is the most commonly used method to date to render water-soluble polymeric gels water-insoluble (irrespective of the pH value of the environment) [9]. This type of polymeric networks offers the possibility to accurately control the release kinetics of incorporated drugs. They are particularly interesting for the delivery of large molecules such as proteins, as the latter can relatively easily diffuse through the hydrogels [5,10]. Importantly, covalent cross-linking leads to the formation of a permanent network with improved mechanical properties of the gel. This is particularly useful for biomedical applications (cell culture support, enzyme immobilization, biomaterial for implants,...) [11]. In the case of drugs that might chemically react with glyoxal

* Corresponding author. Faculté de Pharmacie, Laboratoire de Physique Pharmaceutique, Université Paris-Sud, UMR CNRS 8612, 5 rue Jean-Baptiste Clément, 92296 Châtenay-Malabry Cedex, France. Tel.: +33 1 46 83 56 26; fax: +33 1 46 83 58 82.
E-mail address: florence.agnely@u-psud.fr (F. Agnely).

0939-6411/$ - see front matter © 2007 Elsevier B.V. All rights reserved.
doi:10.1016/j.ejpb.2007.02.012

(*e.g.* proteins), the systems should be loaded with the active agent only after chemical cross-linking and removal of excess free aldehyde. Obviously, the structure of the generated networks (with respect to their cross-linking density and distribution) is a crucial parameter, allowing to accurately control expected functional system properties [12].

Recently, chitosan/poly(ethylene oxide) semi-interpenetrated networks (CS/PEO semi-IPNs) were proposed [13–15]. They consist of the two polymers CS and PEO, which are linked together via physical bonds. In addition, the CS chains are covalently linked upon reaction with glyoxal. Entrapped PEO chains increase the swelling ability of the hydrogels and reinforce the mechanical properties of the systems [14]. A dropping method can be used to prepare these CS/PEO semi-IPN beads [16]. Importantly, the obtained particles are mono-sized, spherical and free-flowing. These are very useful properties for pharmaceutical applications.

Despite the considerable practical importance of the cross-linking of hydrogels with aldehydes, so far only little knowledge is available on the underlying mass transport mechanisms controlling the penetration of cross-linking agents into polymer networks. An interesting study was reported by Hsien and Rorrer [17]. They studied the reaction of glutaraldehyde with chitosan beads. Also Juang et al. investigated this type of beads and cross-linking agent [18]. They found that the cross-linking rate of chitosan with glutaraldehyde could be described by a pseudo-second-order equation and that the cross-linking equilibrium could be quantified by the Freundlich equation. However, the underlying mass transport phenomena and chemical reactions for the cross-linking of hydrogel beads are not yet fully understood, especially if a second polymer, such as PEO is present in the system.

In this study, we aim to better understand the cross-linking process in CS and CS/PEO semi-IPN beads and the resulting polymeric structure of the systems. For this purpose, we measured the uptake kinetics of the cross-linking agent glyoxal into the beads as a function of the glyoxal concentration and bead composition. The results were analyzed using mathematical models based on Fick's second law of diffusion, in order to understand the underlying mass transport mechanisms. We also quantified the amount of glyoxal which had reacted with CS and the amount of unbound glyoxal which is likely to be released from the beads upon administration. This information is very important as glyoxal is considered as toxic [9] and as the hydrogels will therefore require a purification prior to administration.

In addition to this macroscopic analysis, it was of interest to study the distribution of the cross-linking density within the beads. To tackle this point, transversal cross-sections of beads were prepared and analyzed by FTIR microscopy. Because of the small size of the beads (their diameter was about 500–600 μm) [16], it was essential to improve the spatial resolution, in particular to manage to resolve possible heterogeneities from surface to core. That point was reached thanks to synchrotron radiation which offers a brighter source than classical globar sources (around three orders of magnitude) [19]. This emerging instrument is increasingly used in various domains where lateral resolution may be required, for example in pharmacology and in polymer science [20,21]. Using synchrotron radiation, the lateral resolution is no longer limited by the photon flux (20 μm with thermal infrared source) but by the diffraction (half of the wavelength in the infrared domain, extending from 2 to 20 μm, in the mid-infrared). The three parameters – lateral resolution, spectral quality (signal/noise) and dwell time – can be simultaneously optimized, which is essential for the acquisition of highly contrasted and highly detailed 2D images.

2. Materials and methods

2.1. Materials

Chitosan (CS) from crab shells was purchased from Sigma® (Steinheim, Germany). Its average deacetylation degree, determined by FTIR spectroscopy (Impact 420 Nicolet FTIR spectrometer, Nicolet Instrument Corp., USA) using the method described by Brugnerotto et al. [22], was 83%. Its average molar mass, measured by Ubbelohde capillary viscometry [23] (AVS 400 viscometer, Schott-Geräte GmbH, Germany), was 1.6×10^6 g/mol. Poly(ethylene oxide) (PEO, with an average molecular weight of 1.0×10^6 g/mol, according to the manufacturer's specification) was supplied by Aldrich® (Milwaukee, WI, USA). A 40% glyoxal aqueous solution was provided by Acros Organics® (Geel, Belgium). Girard-T reagent ($C_5H_{14}N_3OCl$) from Sigma® (Steinheim, Germany) and sodium tetraborate decahydrate ($Na_2B_4O_7{\cdot}10H_2O$) from Carlo Erba® (Rodano, MI, Italy) were used for the titration reaction of glyoxal. All other reagents used in the experiments were of analytical grade.

2.2. Preparation of the beads

CS was dissolved in a 2% (w/v) acetic acid aqueous solution under gentle stirring for one night (1.5% w/w). This solution was filtered through Whatman ashless filter paper (Whatman Limited, UK). If indicated, PEO was added to the CS solution (at a concentration of 20% w/w, based on the weight of dried CS) for the formation of semi-IPNs [14]. The polymer solutions were dropped into an aqueous sodium hydroxide solution 10% (w/v) under gentle magnetic stirring through a flat-tip needle with an internal diameter of 450 μm (flow rate = 1 ml/min). Since CS is not soluble at high pH, the drops solidified upon polymer precipitation. The obtained beads were collected, were abundantly washed with distilled water to remove residual sodium hydroxide and then they were stored in water. The mean radius of these swollen beads, $\bar{R}$, was determined by transmission optical microscopy (Nikon Eclipse E600, Nikon Corp., Japan) ($n = 100$).

2.3. Measurement of the glyoxal uptake kinetics

To form a covalent network, the CS chains were cross-linked with glyoxal. Twenty grams of the former swollen beads were suspended in 250 ml aqueous glyoxal solutions under mild magnetic stirring. Being a dialdehyde ($C_2H_2O_2$), glyoxal reacts with CS, forming a Schiff base between CS primary amine (amine I) groups and glyoxal aldehyde functions (Fig. 1) [17,24]. The concentration of glyoxal in the cross-linking solution is expressed as the molar ratio "glyoxal molecules:amine groups" ($G:NH_2$). Four different molar ratios were studied: (0.5:1), (1:1), (2:1), and (5:1) corresponding to glyoxal concentrations of 3, 6, 12 and 30 mmol/l, respectively. The ratio (0.5:1) corresponds to the theoretical stoichiometric molar ratio, assuming that one glyoxal molecule (containing two aldehyde functions) is likely to react with two deacetylated monomer units of CS [17].

The beads were exposed to the glyoxal solutions for 24 h under gentle magnetic stirring at 20 °C. The uptake kinetics of the cross-linking agent into the CS and CS/PEO beads were indirectly monitored by measuring the amounts of glyoxal remaining in the surrounding solution as a function of time. At predetermined time points, aliquots were withdrawn and their glyoxal content determined using the UV spectroscopy method described in detail by Mitchel and Birnboim [25] (Beckman DU-70 spectrophotometer; Beckman Coulter, Inc., USA). Briefly, Girard-T reagent ($C_5H_{14}N_3OCl$, 0.1 N) reacts with aldehydic molecules in a weakly basic environment ($Na_2B_4O_7$, 0.5 N, pH 9.2) to form adducts, which strongly absorb UV radiations. In the present case, the concentration of the osazone adduct was measured at $\lambda = 322$ nm. Each experiment was conducted in triplicate. Upon cross-linking, the beads were transferred into a volume $V = 250$ ml of fresh water and stirred for 24 h. The amount of free glyoxal that was released from the beads was assumed to correspond to the amount of unbound glyoxal, and was determined in the water phase as described above. The difference between the total glyoxal amount, on the one hand, and the sum of the amounts of free glyoxal remaining within the cross-linking solution and the free glyoxal released from the beads, on the other hand, was set equal to the amount of glyoxal that reacted with CS amine groups.

2.4. FTIR spectroscopy

FTIR studies were performed on dried beads. Cross-linked beads were dried in a fluidized bed apparatus (Aeromatic-Fielder AG, Switzerland) [16]. Process conditions were as follows: the chamber of the Aeromatic was loaded with 60 g of beads; inlet and outlet temperatures were 38 and 36 °C, respectively; the air flow rate was 2 m^3/min; in addition, compressed air was supplied through a nozzle (top spray) in order to disperse the beads: during the first 15 min a pressure of 2 bars was applied, then 1 bar was maintained for 45 min. Before use, the dried beads were stored in vials at room temperature. The moisture content of these dried beads was 10%, determined by thermogravimetric analysis with a Perkin-Elmer TGA7 (Perkin-Elmer Instruments, USA).

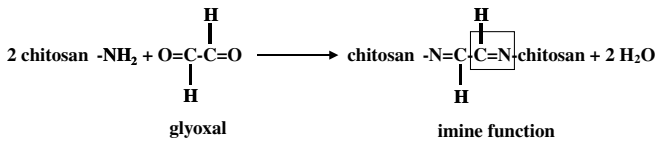

Fig. 1. Cross-linking reaction: formation of a Schiff base.

First, conventional FTIR spectroscopy was conducted on Impact 420 Nicolet FTIR spectrometer equipped with an horizontal ATR accessory (HATR), to validate a quantitative interpretation of the cross-linking intensity as a function of the glyoxal concentration. Beads were previously crushed with a mortar and a pestle. Crushed beads were placed onto the diamond crystal and pressed for an intimate contact. Transmission spectra were collected with 64 scans and a resolution of 4 cm^{-1}.

Second, in order to image the cross-linking density and distribution inside the polymeric beads, synchrotron infrared microspectroscopy (SIRM) was used. The FTIR microscopy station was a Mirage SA5 line SuperAco (Laboratoire d'Utilisation du Rayonnement Electromagnétique, Orsay, France) [26]. The experimental station is equipped with a Nic-Plan IR microscope coupled to a Magna 560 FTIR spectrometer. The microscope operates in confocal mode, where the focusing Schwarzschild objective has a magnification of 32× (NA = 0.65) and the collection Schwarzschild objective a magnification of 10× (NA = 0.71). Analyses were realized through transmission pattern. Fine cross-sections of the beads were obtained by cryomicrotomy using a 5030 Bright cryomicrotome (Bright Instrument Co Ltd., UK). Dried beads were previously molded in an embedding medium (O.C.T., Tissue-Tek®, Sakura, USA). Cross-sections of 4–5 μm thickness were made at −20 °C, and then collected on a ZnS support. Cross-sections were mapped from the periphery to the core, with spot size of 6 × 6 μm. The step size was set to 20 μm to map large areas and reduced to 6 μm to get detailed images of the external regions. IR spectra were collected after 100 scans with an 8-cm^{-1} resolution using Atlμs software (Thermo Nicolet Instruments, USA). Data were analyzed with OMNIC E.S.P. 5.1 software (Nicolet Instrument Corp., USA).

3. Results and discussion

3.1. Glyoxal uptake kinetics

One of the major aims of this work was to monitor and better understand the uptake kinetics of the cross-linking agent glyoxal into CS and CS/PEO semi-IPN beads. In particular, the effects of the initial glyoxal concentration in the cross-linking solution and of the presence/absence

of PEO in the beads on the resulting mass transport phenomena and chemical reactions were to be assessed.

3.1.1. Influence of the initial glyoxal concentration in the cross-linking solution

CS chains, present in the beads as solely polymer network or as semi-IPN together with PEO, were cross-linked. The respective beads were suspended in aqueous glyoxal solutions of different concentrations (and molar G:NH_2 ratios). The glyoxal uptake kinetics were monitored for 24 h. Fig. 2 displays an example of glyoxal uptake kinetics into CS beads for a glyoxal:amine group (G:NH_2) ratio of 0.5:1. The symbols represent the experimentally determined results. Clearly, the glyoxal uptake rate is high at the beginning and then monotonically declines with time. This is a typical feature of diffusion-controlled mass transport phenomena. For this reason, two mathematical models based on Fick's second law of diffusion were fitted to the experimentally determined glyoxal uptake kinetics:

(a) A "complex model" (dotted curve in Fig. 2), considering: (i) the spherical geometry of the beads; (ii) the fact that no glyoxal was present within the polymeric networks at $t = 0$ (before exposure to the cross-linking solution); (iii) glyoxal diffusion with time-independent diffusivities; (iv) the limited volume of the glyoxal solution the beads were exposed to; and (v) decreasing glyoxal concentrations at the interface "bead-cross-linking solution". Considering these initial and boundary conditions, the following analytical solution of Fick's second law of diffusion can be derived [27]:

$$\frac{M_t}{M_\infty} = 1 - \sum_{i=1}^{\infty} \frac{6 \cdot \alpha \cdot (6 \cdot \alpha + 1) \cdot \exp(-D \cdot q_i^2 \cdot t/R^2)}{9 + 9 \cdot \alpha + q_i^2 \cdot \alpha^2} \quad (1)$$

where the q_is are the non-zero roots of:

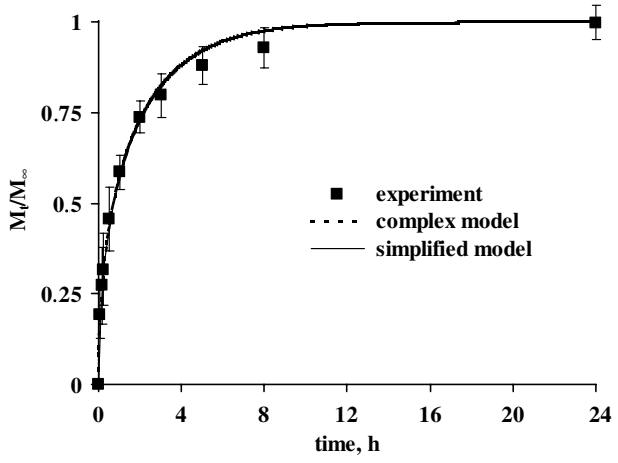

Fig. 2. Glyoxal uptake kinetics into CS beads with a glyoxal:amine group (G:NH_2) ratio of 0.5:1. Experimental data (symbol) and theoretical curves (dotted curve, "complex model of Eq. (1)"; solid curve, "simplified model of Eq. (4)") ($n = 3$).

$$\tan q_i = \frac{3 \cdot q_i}{3 + \alpha \cdot q_i^2} \quad (2)$$

and

$$\alpha = \frac{3 \cdot V}{4 \cdot \pi \cdot R^3} \quad (3)$$

Here, M_t and M_∞ are the cumulative absolute amounts of glyoxal diffused into the beads at time t and infinite time, respectively; D denotes the apparent diffusion coefficient of glyoxal within the beads; R and V represent the radius of the spheres and the volume of the glyoxal solution.

(b) A "simplified model" (solid curve in Fig. 2), which is based on the same assumptions as the "complex model", except for the fact that time-independent glyoxal concentrations are assumed at the interface "bead-cross-linking solution". Under these conditions, the following much less complex equation can be derived quantifying the relative amount of glyoxal taken up into the beads at time t (M_t/M_∞) [27]:

$$\frac{M_t}{M_\infty} = 1 - \frac{6}{\pi^2} \cdot \sum_{i=1}^{\infty} \frac{1}{i^2} \cdot \exp\left(-\frac{D \cdot i^2 \cdot \pi^2 \cdot t}{R^2}\right) \quad (4)$$

where D denotes the constant diffusion coefficient of glyoxal within the hydrogels and R the radius of the spheres, respectively. The amount of diffused glyoxal (in mmol) as a function of time can therefore be fitted with the following equation:

$$M_t = M_\infty \cdot \left(1 - \frac{6}{\pi^2} \cdot \sum_{i=1}^{\infty} \frac{1}{i^2} \cdot \exp\left(-\frac{D \cdot i^2 \cdot \pi^2 \cdot t}{R^2}\right)\right) \quad (5)$$

In our experiments M_∞ was the cumulative amount of diffused glyoxal at time $t = 24$ h.

As it can be seen in Fig. 2, good agreement between these theories (curves) and the experimentally determined glyoxal uptake kinetics (symbols) was observed, irrespective of the type of mathematical model. This can serve as an indication that glyoxal penetration is primarily controlled by diffusion through the hydrogel-based beads and that changes in the glyoxal concentration at the interface "bead-cross-linking solution" are negligible. As the two theories resulted in almost identical uptake kinetics, only the "simplified model" was used for further analysis.

However, it has to be pointed out that glyoxal diffusion into the spheres is not the only process that takes place. The chemical reaction of this cross-linking agent with amine groups of CS also occurs. The good agreement between the presented diffusion models and the experimentally determined glyoxal uptake kinetics (Fig. 3) can serve as an indication that the rate of the cross-linking reaction (Fig. 1) is much higher than the diffusion rate of glyoxal within the investigated beads. As both processes occur sequentially, the slower one (diffusion) controls the overall penetration kinetics.

Importantly, the two mathematical models assume time-independent diffusion coefficients (*e.g.*, a diffusion coeffi-

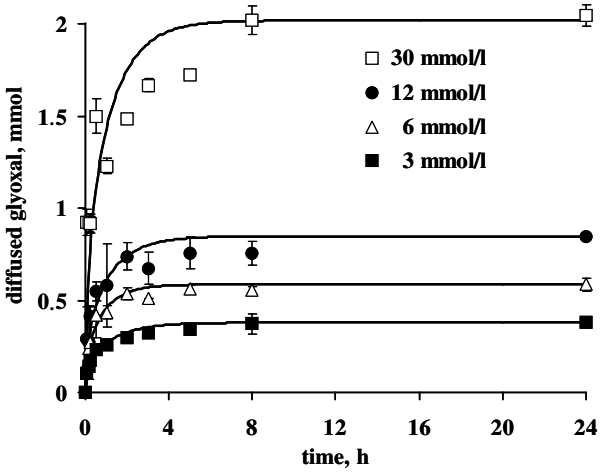

Fig. 3. Effects of the glyoxal concentration in the cross-linking solution (indicated in the figure) on the uptake kinetics of the cross-linking agent into CS beads. Experimental data (symbols) and theoretical curves ("simplified model of Eq. (5)") ($n = 3$).

cient of $(1.6 \pm 0.4) \times 10^{-7}$ cm^2/s was determined for the glyoxal:amine group ratio 0.5:1; Fig. 2). Thus, their good agreement with the experimental results indicates that the mobility of glyoxal within the beads does not significantly change with time during the observation period. Consequently, the mesh size of the investigated hydrogels (before and after cross-linking) can be expected to be much larger than the hydrodynamic diameter of the cross-linking agent ($MW_{glyoxal} = 58$ g/mol). In addition, a homogeneous cross-linking density distribution throughout the beads can be expected.

The effects of the glyoxal concentration in the cross-linking solution on the resulting glyoxal uptake kinetics are illustrated in Fig. 3. Clearly, the absolute uptake rate and extent increased with increasing glyoxal concentration. However, the apparent diffusion coefficient of the cross-linking agent in the polymeric networks was not significantly altered, varying between $(1.6 \pm 0.6) \times 10^{-7}$ cm^2/s and $2.5\ (\pm 1.6) \times 10^{-7}$ cm^2/s (Table 1). This is a further indication for the fact that the mesh sizes of the polymeric networks are likely to be much larger than the glyoxal molecules. Based on this knowledge, it is possible to predict in a quantitative way how much glyoxal diffuses into the hydrogel beads at arbitrary cross-linking concentrations in the bulk solution.

Table 1
Measured radius $\bar{R}$ and glyoxal diffusion coefficient $\bar{D}$ (mean ± standard deviation, $n = 3$) in CS and CS/PEO semi-IPN beads at 20 °C for different theoretical (G:NH_2) ratios

Polymer	Theoretical (G:NH_2) ratio	$\bar{R}$ (μm)	$\bar{D}$ (10^{-7} cm^2/s)
CS	0.5:1	865 ± 30	1.6 ± 0.4
	1:1	865 ± 30	2.2 ± 0.3
	2:1	865 ± 30	2.5 ± 1.6
	5:1	865 ± 30	1.6 ± 0.6
CS/PEO	0.5:1	825 ± 15	0.8 ± 0.2
	5:1	825 ± 15	n.d.

$\bar{D}$ is derived from the fitting of Eq. (5) to the experimental data.
n.d., non-determined.

3.1.2. Effect of the presence of PEO chains within the CS network

According to Table 1, the apparent diffusion coefficients of the cross-linking agent in CS beads and in CS/PEO semi-IPN beads were equal to $\bar{D} = (1.6 \pm 0.4) \times 10^{-7}$ cm^2/s and $\bar{D} = (0.8 \pm 0.2) \times 10^{-7}$ cm^2/s, respectively. It appears that the presence of PEO slightly decreased the apparent diffusion coefficient of glyoxal within the polymeric network due to the obstruction effect of the additional PEO chains. Yet, for the same mass of chitosan, the absolute amounts of aldehyde that diffused into the beads at equilibrium (24 h) were not altered by addition of PEO (see Fig. 4) since this polymer does not chemically react with glyoxal. Thus, the resulting cross-linking density is likely to be similar in both systems.

3.1.3. Yield of the cross-linking reaction

After 24 h in contact with the cross-linking solution, polymer beads were resuspended in water in order to quantify the amount of free glyoxal released from the beads, *i.e.* the amount of glyoxal which did not chemically react with CS. The different glyoxal amounts (in the initial cross-linking solution, in the cross-linking solution after 24 h, of free glyoxal released from the beads and of bound glyoxal) are listed in Table 2. As residual free glyoxal is toxic, a rigorous washing procedure of the cross-linked beads allowing to reduce the aldehyde content below the authorised limit will be required prior to administration to humans. From the glyoxal amounts in Table 2, the yield of the cross-linking reaction could be calculated, as well as the effective (G:NH_2) ratio. Table 3 shows yield values, as percentages of reacted glyoxal, and the theoretical and effective

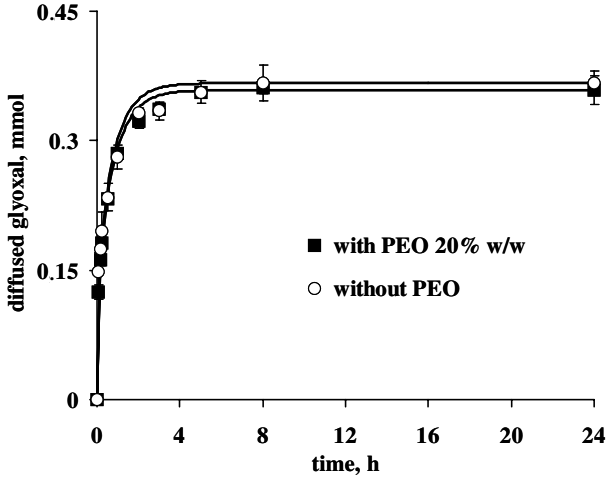

Fig. 4. Influence of the presence of PEO within the CS beads on the glyoxal uptake kinetics (glyoxal:amine group ratio, 0.5:1). Experimental data (symbols) and theoretical curves ("simplified model of Eq. (5)") ($n = 3$).

Table 2
Initial glyoxal amount in the cross-linking solution, residual glyoxal amount in the cross-linking solution after 24 h, released glyoxal amount and bound glyoxal amount for cross-linked CS and CS/PEO semi-IPN beads (means ± standard deviation, $n = 3$)

Polymer	Theoretical ($G:NH_2$) ratio	Initial glyoxal amount (10^{-5} mol/g of beads)	Residual glyoxal amount (10^{-5} mol/g of beads)	Released glyoxal amount (10^{-5} mol/g of beads)	Bound glyoxal amount (10^{-5} mol/g of beads)
CS	0.5:1	3.82	1.9 ± 0.1	0.41 ± 0.04	1.4 ± 0.2
	1:1	7.65	4.7 ± 0.2	0.8 ± 0.1	2.1 ± 0.2
	2:1	15.0	10.73 ± 0.07	1.54 ± 0.01	2.7 ± 0.1
	5:1	37.4	27 ± 1	3.1 ± 0.4	6 ± 1
CS/PEO	0.5:1	3.82	1.89 ± 0.09	0.42 ± 0.01	1.5 ± 0.1
	5:1	37.4	31.0 ± 0.3	0.43 ± 0.07	5.9 ± 0.4

Table 3
Characteristics of the obtained cross-linked CS and CS/PEO semi-IPN beads: theoretical and effective ($G:NH_2$) ratios, cross-linking reaction yields and average molar masses M_C between two cross-links (means ± standard deviation, $n = 3$)

Polymer	Theoretical ($G:NH_2$) ratio	Effective ($G:NH_2$) ratio	Yield (%)	M_C (g/mol)
CS	0.5:1	0.19 (±0.02):1	39 ± 4	640 ± 120
	1:1	0.27 (±0.02):1	27 ± 3	340 ± 70
	2:1	0.36 (±0.01):1	18.1 ± 0.4	160 ± 10
	5:1	1.0 (±0.2):1	19 ± 4	n.d.
CS/PEO	0.5:1	0.20 (±0.01):1	40 ± 2	620 ± 60
	5:1	0.79 (±0.04):1	15.8 ± 0.9	n.d.

n.d., non-determined.

($G:NH_2$) ratios, corresponding to different kinds of beads (based on CS and CS/PEO semi-IPN). Importantly, there is no significant difference between CS beads and CS/PEO semi-IPN beads (at the same initial glyoxal concentration). In particular, the CS cross-linking extent does not seem to be affected by the presence of the PEO.

Another way to express the yield of the cross-linking reaction is to estimate the average molar mass of the CS chains between two cross-links (denoted as M_C). As shown in Table 3, the effective ($G:NH_2$) molar ratio appears in the form α:1, *i.e.* 1 mole of glyoxal for $\frac{1}{\alpha}$ mole of NH_2. Assuming that one molecule of glyoxal reacts with two amine groups, $(\frac{1}{\alpha} - 2)$ free amine groups remain. Considering the average deacetylation degree of CS, there are 83% deacetylated monomer units and 17% acetylated monomer units in the polymer chains. Thus, between two cross-links, CS chains present $(\frac{1}{\alpha} - 2)$ deacetylated monomer units and $(\frac{1}{\alpha} - 2) \times \frac{17}{83}$ acetylated monomer units. Hence, the average molar mass of the CS chains between two cross-links (M_C) can be calculated as follows:

$$M_C = \left(\frac{1}{\alpha} - 2\right) \times M_{DEAC} + \left(\frac{1}{\alpha} - 2\right) \times \frac{17}{83} \times M_{AC} \qquad (6)$$

where $M_{DEAC} = 161.2$ g/mol and $M_{AC} = 203.2$ g/mol are the molar masses of deacetylated and acetylated monomer units, respectively. The obtained M_C values are average values and assume a relatively homogeneous cross-linking density throughout the beads.

When the ($G:NH_2$) ratio increases, the amount of bound glyoxal increases (see Table 2) and the average length of the CS chains between two cross-links decreases (see Table 3), indicating that the mesh of the covalent network tightens. However, when glyoxal is present in excess [theoretical ratio (5:1)], M_C becomes a negative value and does not have a signification anymore. From a physical point of view, such a negative value reveals that both aldehyde functions of the glyoxal molecules do not necessarily react with CS, compromising the creation of the three-dimensional covalent network.

Importantly, the M_C values obtained for CS and CS/PEO semi-IPN beads do not significantly differ (Table 3), confirming the similar structures of the CS covalent networks in both types of systems.

3.2. Cross-linking density distribution

3.2.1. Quantitative study of cross-linking reaction by conventional FTIR spectroscopy

As many organic compounds, CS presents a characteristic absorption in the IR domain [22]. At 1650 cm^{-1}, its spectrum shows a band corresponding to an amide function, *i.e.* acetylated amine, whereas the band at 1590 cm^{-1} corresponds to a free amine I function, *i.e.* deacetylated amine. When CS is chemically cross-linked with glyoxal, the aldehyde reacts with the amine I functions to give a Schiff base, creating covalent bridges between the polymer chains. Fig. 5 shows the IR spectra of cross-linked CS and non-cross-linked CS. The amide amount is not affected during cross-linking of CS, hence the band intensity at 1650 cm^{-1} was considered as an internal reference. In contrast, intensity of the amine I band at 1590 cm^{-1} is clearly altered. Fig. 6 shows the decrease of the amine I band intensity with increasing molar ($G:NH_2$) ratio.

It is, thus, possible to follow the disappearance of the amine I functions during the cross-linking reaction, monitoring the decrease in the ratio between the amine I band area and the amide band area, the latter remaining unaltered. This ratio is denoted $R_{I/II}$. $R_{I/II}$ is calculated taking the line passing through the points of the spectrum situated at 750 cm^{-1} and at 1780 cm^{-1} as the baseline. The area of the amine I band was calculated over the interval between 1585 and 1595 cm^{-1}, whereas the area of the amide band was calculated over the interval between 1645 and 1655 cm^{-1}. Fig. 7 represents the dependence of $R_{I/II}$ on the molar ($G:NH_2$) ratio. Clearly, the $R_{I/II}$ value decreases

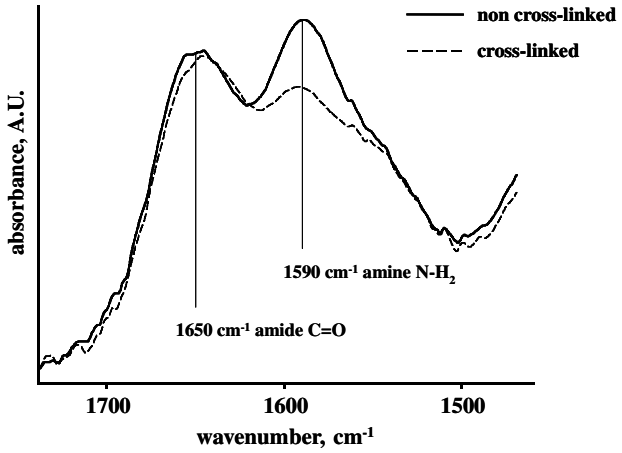

Fig. 5. IR spectra of non-cross-linked and cross-linked CS.

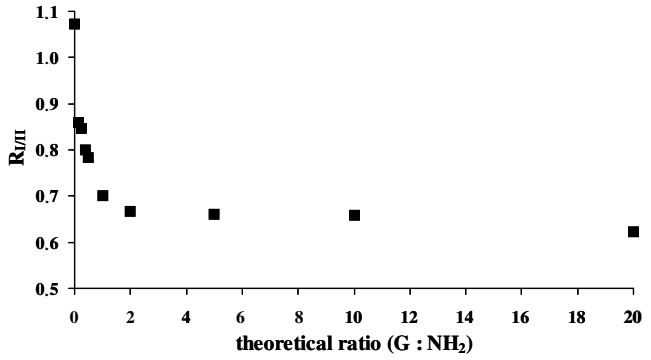

Fig. 7. Dependence of the $R_{I/II}$ value on the molar ($G:NH_2$) ratio within CS beads.

with increasing ($G:NH_2$) ratio. However, above a glyoxal concentration corresponding to the molar ratio (2:1), $R_{I/II}$ remains about constant, indicating that the cross-linking has reached its maximum intensity.

Thus, a relative quantification of the cross-linking reaction could be obtained based on changes in the $R_{I/II}$ values. However, using this indicator the cross-linking reaction is only indirectly and partially quantified; it primarily informs about the engagement of the amine I functions in the formation of the Schiff base with glyoxal. That is why, it does not inform about the effective creation of bridges between two different CS chains. Thus, the analysis does not allow us to evaluate whether the two aldehyde functions of the glyoxal molecules actually reacted (effective cross-links) or not. Hence, the following discussion about the cross-linking density relies on the hypothesis that glyoxal reacts to form an effective CS network. This hypothesis is justified for molar ratios ($G:NH_2$) below (2:1).

The influence of the presence of PEO within the polymer network was also evaluated in this study. CS beads were prepared with five different PEO concentrations: 0%, 10%, 20%, 35% and 50% w/w (referring to the dry weight of CS). The beads were analyzed by standard FTIR spectroscopy. It has to be pointed out that the PEO infrared spectrum does not interfere in the considered wave-number domain. The evolution of the $R_{I/II}$ value as a function of the PEO percentage within the beads seems to indicate that PEO did not have any significative effect on the final cross-linking density, irrespective of the glyoxal concentration [theoretical ratios (0.5:1) and (2:1)] (Fig. 8). The $R_{I/II}$ mean value and standard deviation, calculated over the five PEO concentrations, were $R_{I/II} = 1.04 \pm 0.03$ for non-cross-linked beads. Considering that PEO does not react with amine I functions of CS, in the absence of glyoxal the observed standard deviation is due to the measurement error. For the cross-linked beads, the $R_{I/II}$ mean value and standard deviation were $R_{I/II} = 0.77 \pm 0.02$ and $R_{I/II} = 0.67 \pm 0.02$ at the ($G:NH_2$) ratios (0.5:1) and (2:1), respectively.

3.2.2. Imaging of the cross-linking density and distribution by SIRM

SIRM allows to get 2D chemical images by acquiring infrared spectra at each pixel of the desired map. Thus, monitoring changes in the $R_{I/II}$ value (indicating the number of residual amine I functions), we could image the

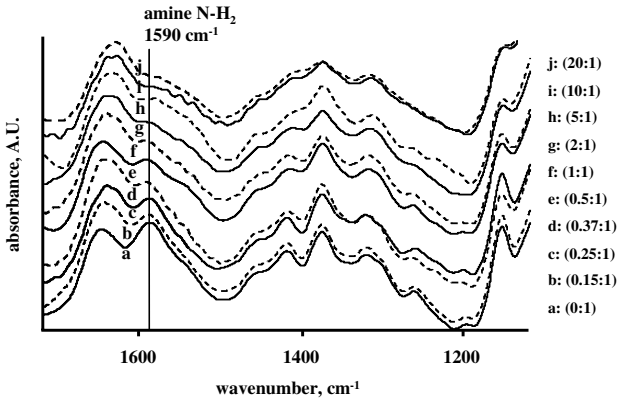

Fig. 6. IR spectra of non-cross-linked CS (0:1) and cross-linked CS with increasing amounts of glyoxal [the molar ($G:NH_2$) ratio varies from (0.15:1) to (20:1) as indicated].

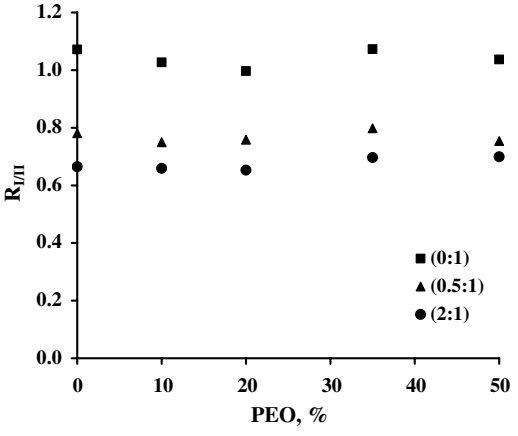

Fig. 8. Dependence of the $R_{I/II}$ value on the PEO content within CS beads with increasing amounts of glyoxal [the molar ($G:NH_2$) ratio varies from (0:1) to (2:1) as indicated].

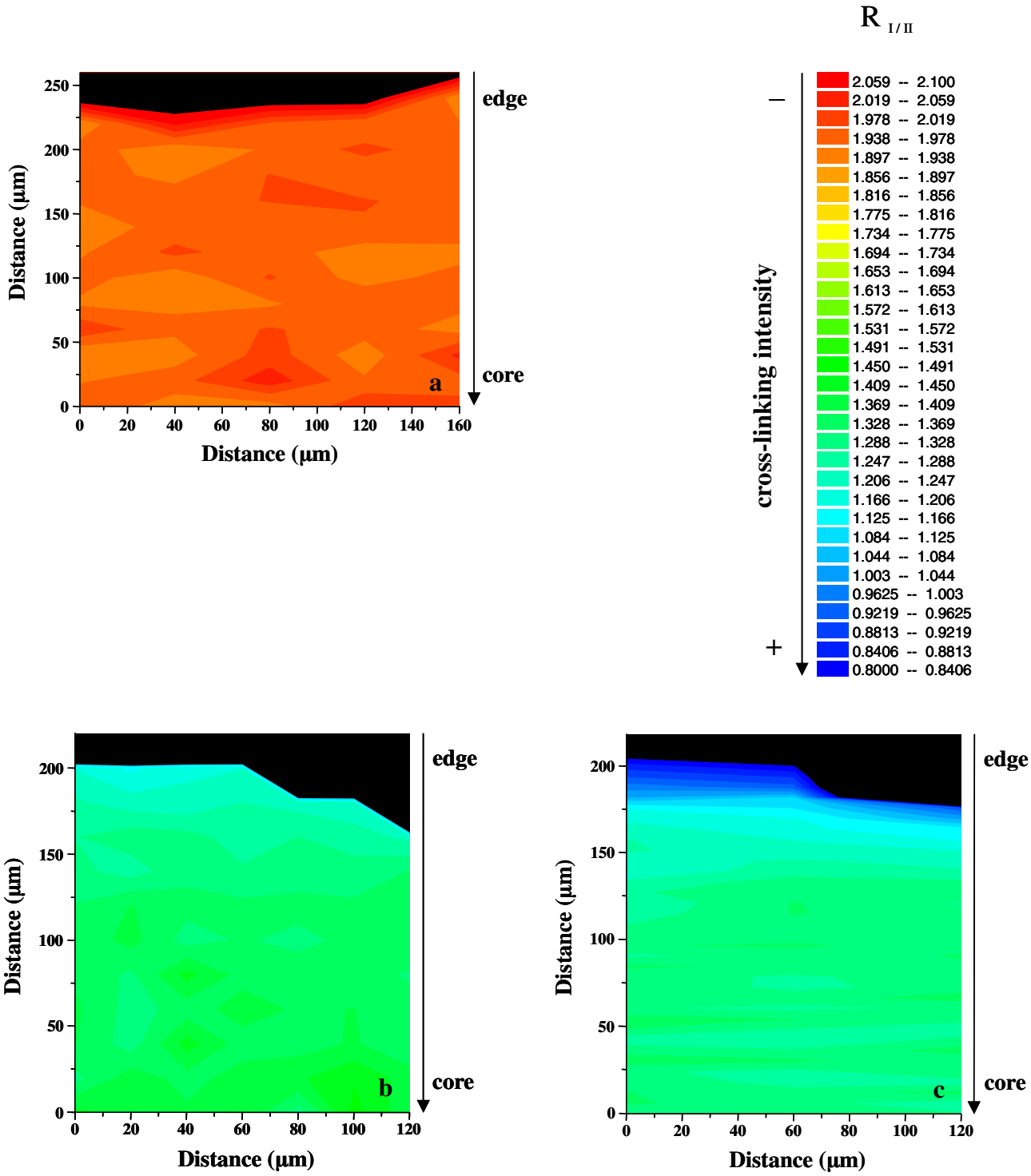

Fig. 9. Maps of cross-sections of CS beads measured by SIRM: effects of the glyoxal concentration on the $R_{I/II}$ value in: (a) non-cross-linked CS beads [molar (G:NH_2) ratio (0:1)], (b) cross-linked CS beads [molar (G:NH_2) ratio (0.5:1)], and (c) cross-linked CS beads [molar (G:NH_2) ratio (2:1)].

samples in terms of cross-linking density and distribution. The embedding medium used for microtomy (OCT) does not absorb in this energy domain, so the precedent discussion on the quantitative aspects of the cross-linking reaction based on FTIR spectroscopy is still valid.

Fig. 9 shows the maps obtained by SIRM measurements of cross-sections of polymeric beads (from the periphery to the core). These maps indicate the variations of the cross-linking density as a function of the position and of the molar (G:NH_2) ratio.

Red–orange zones correspond to regions with high $R_{I/II}$ values, indicating that the CS chains present numerous free amine I groups (as in the case of non-cross-linked CS beads: Fig. 9a). In contrast, green and blue zones corre-

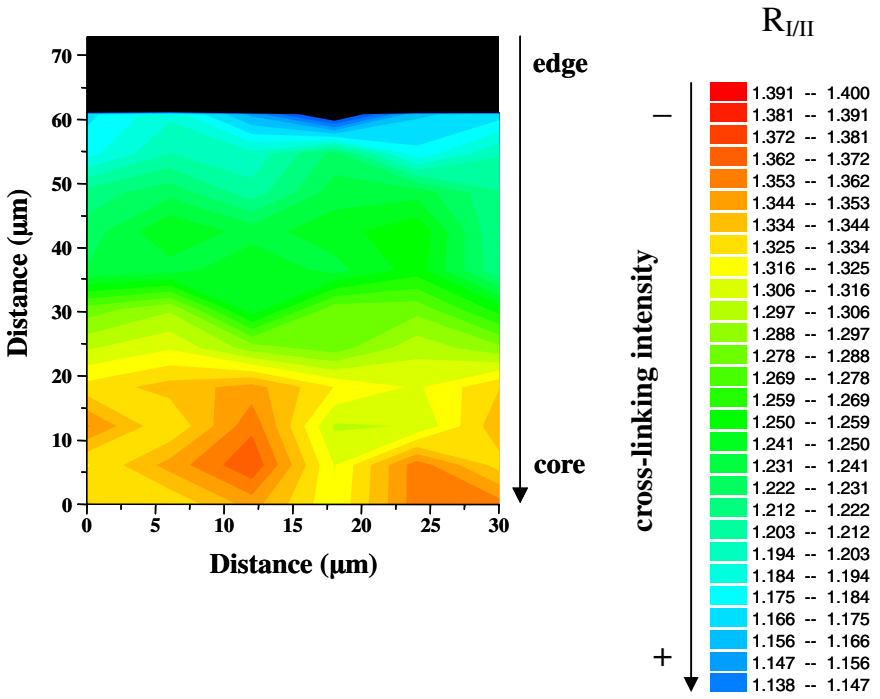

Fig. 10. Map of a cross-section of a cross-linked CS bead measured by SIRM: zoom on the periphery (60 μm) [molar (G:NH_2) ratio (0.5:1)].

spond to regions with smaller $R_{I/II}$ values, indicating lower amounts of free amine I groups compared to amide groups. Comparing Fig. 9b and c, it becomes obvious that the cross-linking density in CS beads with a molar (G:NH_2) ratio of (2:1) is higher than in the corresponding beads with a molar (G:NH_2) ratio of (0.5:1) (more blue colour in Fig. 9c compared to Fig. 9b, especially at the edge; same colour scale and same experimental conditions).

It has to be pointed out that the $R_{I/II}$ values are relative values and do not have any physical signification. They only allow to compare maps obtained under the same conditions with each other. That is why the present analysis of the cross-linking density is semi-quantitative, and not quantitative. If the intensity values obtained in these maps are compared to those obtained with conventional FTIR spectroscopy (Fig. 7), they do not exactly correspond. With conventional FTIR spectroscopy, $R_{I/II}$ values in the range of 1.9–2 indicate the absence of cross-linking, whereas with SIRM (Fig. 9), non-cross-linked regions are indicated by a $R_{I/II}$ value of around 1.1. The latter values were obtained in the transmission mode with a synchrotron spectrometer and the first type of values in the ATR mode with a conventional FTIR spectrometer. From one configuration to another, optical responses may differ for the same sample. These differences are for example due to differences in the geometry of the device, tolerance of the filters, sensitivity of detectors, *etc*. [28].

Interestingly, the cross-linking is not homogeneous over the whole cross-section of the beads (periphery/core) (Fig. 9b and c). There is a region located at the surface of the beads (periphery of the cross-sections), where the cross-linking appears to be more intense. Fig. 10 shows a map zooming on the edge of a cross-section of a cross-linked CS bead. Clearly, there is a gradient of the $R_{I/II}$ value over the region of 20–30 μm from the surface towards the core of the beads. The colour scale was adjusted in order to better visualize the cross-linking density gradient. In any case, glyoxal appears to have diffused up to the core of the beads, confirming the results of the glyoxal diffusion studies.

4. Conclusions

In this work, the interpretation of the glyoxal uptake kinetics within CS and semi-IPN beads allowed to better understand the underlying mass transport processes within these systems. The influence of the initial glyoxal concentration in the cross-linking solution and the effects of the presence/absence of PEO within the CS network were studied. Mathematical modeling of the observed glyoxal uptake kinetics, using Fick's second law of diffusion, showed that glyoxal transport within the polymeric beads was primarily controlled by pure diffusion with concentration- and time-independent diffusion coefficients. Importantly, the cross-linking reaction was found to be unaltered by the presence of PEO within CS network. The amounts of unbound, bound and free glyoxal were also determined. All this obtained knowledge can be very useful for the optimizing of the preparation of these types of beads (*e.g*. with respect to the duration of the cross-linking process and with respect to the washing procedure that will be required to remove free glyoxal molecules prior to administration).

The use of synchrotron infrared microspectroscopy proved to be very powerful for the analysis of the microstructures of the resulting polymeric networks. Maps of cross-sections of cross-linked beads confirmed that glyoxal diffused through the entire system, irrespective of the glyoxal concentration. Moreover, the high-resolution images revealed that cross-linking was more intense within an outer shell of about 30 μm next to the surfaces of the beads. This information on the three-dimensional structures of the polymer networks will be of great help for the design of innovative drug delivery systems. Indeed, the cross-linking density and distribution elucidated in this paper will certainly affect the swelling properties of the hydrogels and, thus, the resulting drug release kinetics.

References

[1] T. Chandy, C.P. Sharma, Biodegradable chitosan matrix for the controlled release of steroids, Biomater. Artif. Cells Immobilization Biotechnol. 19 (4) (1991) 745–760.
[2] S.B. Rao, C.P. Sharma, Use of chitosan as a biomaterial: studies on its safety and hemostatic potential, J. Biomed. Mater. Res. 34 (1997) 21–28.
[3] R.A.A. Muzzarelli, in: R.A.A. Muzzarelli (Ed.), Chitin, Pergamon Press, Oxford, 1977.
[4] R. Shepherd, S. Reader, A. Falshaw, Chitosan functional properties, Glycoconj. J. 14 (4) (1997) 535–542.
[5] L. Illum, Chitosan and its use as pharmaceutical excipient, Pharm. Res. 15 (9) (1998) 1326–1331.
[6] S. Hirano, Chitin and chitosan as novel biotechnological materials, Polym. Int. 48 (8) (1999) 732–734.
[7] T. Chandy, C.P. Sharma, Chitosan matrix for oral sustained delivery of ampicillin, Biomaterials 14 (12) (1993) 939–944.
[8] K.C. Gupta, M.N.V. Ravi Kumar, Drug release behavior of beads and microgranules of chitosan, Biomaterials 21 (2000) 1115–1119.
[9] J. Berger, M. Reist, J.M. Mayer, O. Felt, N.A. Peppas, R. Gurny, Structure and interactions in covalently and ionically crosslinked chitosan hydrogels for biomedical applications, Eur. J. Pharm. Biopharm. 57 (1) (2004) 19–34.
[10] F.L. Mi, C.Y. Kuan, S.S. Shyu, S.T. Lee, S.F. Chang, The study of gelation kinetics and chain-relaxation properties of glutaraldehyde-cross-linked chitosan gel and their effects on microspheres preparation and drug release, Carbohyd. Polym. 41 (2000) 389–396.
[11] R.S. Juang, F.C. Wu, R.L. Tseng, Use of chemically modified chitosan beads for sorption and enzyme immobilization, Adv. Environ. Res. 6 (2) (2002) 171–177.
[12] N.A. Peppas, Preparation methods and structure of hydrogels, in: N.A. Peppas (Ed.), Hydrogels in Medicine and Pharmacy. Fundamentals, vol. 1, CRC Press, Boca Raton, 1986, pp. 1–25.
[13] V.R. Patel, M.M. Amiji, Preparation and characterization of freeze-dried chitosan-poly(ethylene oxide) hydrogels for site-specific antibiotic delivery in the stomach, Pharm. Res. 13 (4) (1996) 588–593.
[14] M.N. Khalid, L. Ho, F. Agnely, J.L. Grossiord, G. Couarraze, Swelling properties and mechanical characterization of a semi-interpenetrating chitosan/polyethylene oxide network. Comparison with a chitosan reference gel, S.T.P. Pharma. Sci. 9 (4) (1999) 359–364.
[15] M.N. Khalid, F. Agnely, N. Yagoubi, J.L. Grossiord, G. Couarraze, Water state characterization, swelling behavior, thermal and mechanical properties of chitosan based networks, Eur. J. Pharm. Sci 15 (5) (2002) 425–432.
[16] L.M. Martinez, F. Agnely, R. Bettini, M. Besnard, P. Colombo, G. Couarraze, Preparation and characterization of chitosan based micro networks: transposition to a prilling process, J. Appl. Polym. Sci. 93 (2004) 2550–2558.
[17] T.Y. Hsien, G.L. Rorrer, Heterogeneous cross-linking of chitosan gel beads: kinetics, modeling, and influence on cadmium ion adsorption capacity, Ind. Eng. Chem. Res. 36 (9) (1997) 3631–3638.
[18] R.-S. Juang, F.-C. Wu, R.-L. Tseng, Solute adsorption and enzyme immobilization on chitosan beads prepared from shrimp shell wastes, Bioresour. Technol. 80 (3) (2001) 187–193.
[19] P. Dumas, L. Miller, The use of synchrotron infrared microspectroscopy in biological and biomedical investigations, Vib. Spectrosc. 32 (2003) 3–21.
[20] M. Cotte, P. Dumas, M. Besnard, P. Tchoreloff, P. Walter, Synchrotron FT-IR microscopic study of chemical enhancers in transdermal drug delivery: example of fatty acids, J. Control. Release 97 (2) (2004) 269–281.
[21] G. Ellis, C. Marco, M. Gomez, Highly resolved transmission infrared microscopy in polymer science, Infrared Phys. Technol. 45 (5–6) (2004) 349–364.
[22] J. Brugnerotto, J. Lizardi, F.M. Goycoolea, W. Argüelles-Monal, J. Desbrières, M. Rinaudo, An infrared investigation in relation with chitin and chitosan characterization, Polymer 42 (8) (2001) 3569–3580.
[23] G.A.F. Roberts, J.G. Domszy, Determination of the viscometric constants for chitosan, Int. J. Biol. Macromol. 4 (6) (1982) 374–377.
[24] G.A.F. Roberts, K.E. Taylor, Chitosan gels. Part 3. The formation of gels by reaction of chitosan with glutaraldehyde, Makromol. Chem. 190 (1989) 951–960.
[25] R.E.J. Mitchel, H.C. Birnboim, The use of Girard-T reagent in a rapid and sensitive method for measuring glyoxal and certain other α-dicarbonyl compounds, Anal. Biochem. 81 (1) (1977) 47–56.
[26] F. Polack, R. Mercier, L. Nahon, C. Armellin, J.P. Marx, M. Tanguy, M.E. Couprie, P. Dumas, Optical design and performance of the IR microscope beamline at SUPERACO-France, in: G.L. Carr, P. Dumas (Eds.), SPIE, 3775, 1999, pp. 13–21.
[27] J. Crank, in: The Mathematics of Diffusion, second ed., Clarendon Press, Oxford, 1975.
[28] P. Leroux, in: Guide de l'utilisateur de spectromètres d'absorption dans le proche infrarouge, Bipea, Gennevilliers, 1996.